



Photoionization of the formyl radical using the *B*-spline *R*-matrix method

Kedong Wang ^{*}, Haiyang Qiao, Jie Liu, Yan Wang, Haoxing Zhang, and Yufang Liu
School of Physics, Henan Normal University, Xinxiang, 453007, People's Republic of China

 (Received 4 January 2022; accepted 6 April 2022; published 19 April 2022)

There are major discrepancies between recent [J. D. Savee *et al.*, *J. Phys. Chem. A* **125**, 3874 (2021)] and the two early [B. L. FitzPatrick *et al.*, *J. Chem. Phys.* **133**, 094306 (2010); V. A. Shubert and S. T. Pratt, *J. Phys. Chem. A* **114**, 11238 (2010)] measurements regarding an absolute cross section for the photoionization of formyl radicals. To estimate the accuracy of the various results, we carried out calculations with the *R*-matrix method employing the configuration-interaction method to describe electronic correlation. The quality of the description of the continuum is assessed by using the Gaussian, *B*-spline, and their mixed bases. The convergence of the results is checked by changing the partial waves and active spaces. Accurate cross sections and asymmetry parameters for the valence orbitals are reported for photon energies from the ionization thresholds to 90 eV. Extensive resonance structures are observed near the ionization threshold.

DOI: [10.1103/PhysRevA.105.042811](https://doi.org/10.1103/PhysRevA.105.042811)

I. INTRODUCTION

The response of atomic systems to ionizing radiation is a dominant process in the universe. It involves neutral atoms, molecules, and clusters, as well as their ions, and takes place in many physical systems including a variety of astrophysical objects, the upper atmosphere, fission, and fusion plasmas, as well as laser-produced plasmas. In many cases, the role of the photoionization (PI) process is central in determining the overall properties of a system. Despite significant experimental and theoretical progress over the last two decades in the understanding of the PI process at low collision energies, there still remain many open questions, specifically in the case of polyatomic molecules. Indeed, the theoretical treatment of polyatomic molecules is especially difficult because PI itself is a highly correlated process. In the present study, we reported the PI cross sections and asymmetry parameters for the HCO radical.

Absolute PI cross sections of reactive radicals are far less well known than those of stable molecules. The ephemeral nature of radicals is chiefly responsible for making their detection difficult. Experimental measurements concerning PI cross sections of HCO radicals are difficult to perform, because the absolute concentration of radicals is difficult to measure. Given that the formyl radical is a prototypical triatomic free radical of importance in combustion [1], atmospheric chemistry [2], and interstellar space [3], the investigation of properties related to its spectrum has attracted much attention. Three experimental works for the PI of HCO radicals can be found in the literature. Shubert and Pratt [4] determined the absolute PI cross section of HCO by using the laser-based VUV PI and the imaging method, along with the known absolute PI cross section of CH₃. They used the photodissociation of CH₃CHO to produce CH₃ and HCO. This spectrum

agrees with a later one from FitzPatrick *et al.* [5], who determined the absolute PI cross section by a different method. They employed a crossed laser molecular beam apparatus coupled with undulator-generated tunable VUV radiation to create a 1:1 ratio of C₂H₄ and HCO from the secondary dissociation of C₃H₅O fragments, and set it to an absolute cross-section scale using the well-known cross section for ethene at 11.27 eV. Recently, Savee *et al.* [6] measured a PI spectrum of the HCO radical between 8 and 11.5 eV. They use two independent methods, photodissociation of acetaldehyde and the Cl + H₂CO reaction, to produce the ubiquitous HCO and measure its PI spectrum and absolute PI cross section. However, the resulting cross-section values from Savee *et al.* [6] are a factor of 2 larger than those determined from the measurements of FitzPatrick *et al.* [5], and a factor of 1.5 larger than those of Shubert and Pratt [4].

The principal motivation for the present work, therefore, was to shed more light on the ongoing discussion by performing an accuracy calculation for PI from HCO radicals. The calculations were performed with the *R*-matrix method [7], which employed the configuration-interaction (CI) method to describe the electronic correlation. The distinctive feature of the method is to allow the use of *B*-spline type orbitals (BTOs) to generate accurate descriptions of the continuum. This approach has proved to be reliable in PI studies on radicals such as OH [8] and CH [9].

As reported above, PI cross-section measurements in HCO radicals are limited to photon energies of about 3 eV above the ionization threshold. A theoretical PI cross section of HCO is needed. Hence, the second goal of the present work is to provide the PI cross-section profile for the outermost orbital of HCO over a more extended photon energy range (up to 90 eV). It is also the purpose of this study to detect resonances and autoionization processes, which appear at the PI spectra near threshold.

This paper is organized as follows. Section II describes the computational method for the structure and the

^{*}wangkd@htu.cn

PI processes. Some tests of various models for the studied PI cross section are described in Sec. III. This is followed by a presentation of the final result and discussion in Sec. IV, and finally the conclusions in Sec. V.

II. COMPUTATIONAL DETAILS

A. Theoretical method

In the present paper, the bound and the continuum wave functions in PI calculations are presented with an R -matrix calculation. The R -matrix method [10] employed here is based on the division of space into an internal region containing all of the N -electron target charge cloud and an external scattering region. In the inner region, both the initial and final states are given in terms of the basis functions ψ_k^N as

$$\Phi_i^N = \sum_k B_{ik} \psi_k^N(x_1, \dots, x_N), \quad (1)$$

$$\Psi_f^{(-)N}(k_f) = \sum_k A_{fk}^{(-)}(k_f) \psi_k^N(x_1, \dots, x_N), \quad (2)$$

where $A_{fk}^{(-)}(k_f)$ and B_{ik} are energy-dependent expansion coefficients determined from matching the wave functions (2) and (1) to the well-known asymptotic solutions of the system, and x_i stands for the space-spin coordinates of the i th electron. The R -matrix basis functions ψ_k^N in turn are written in the close-coupling form

$$\begin{aligned} \psi_k^N(x_1, \dots, x_N) = & \mathcal{A} \sum_{ij} a_{ijk} \Phi_i^{N-1}(x_1, \dots, x_{N-1}) \eta_{ij}(x_N) \\ & + \sum_p b_{kp} \chi_p^{(N)}(x_1, \dots, x_N). \end{aligned} \quad (3)$$

Here, η_{ij} are the continuum orbitals orthogonalized with respect to the target orbitals, and \mathcal{A} is an antisymmetrization operator. Coefficients a_{ijk} and b_{kp} are variational parameters determined by the matrix diagonalization. The summation in the second term of Eq. (3) runs over configurations χ_p , where all electrons are placed in target-occupied and virtual molecular orbitals. The choice of appropriate χ_p is crucial. These are L^2 configurations and are needed to account for polarization and for correlation effects arising from excitations in the neutral molecule.

Using the bound and the continuum wave functions obtained above, the PI cross sections in the length gauge are given in the form [11,12]

$$\frac{d\sigma_{if}}{dk_f} = 4\pi^2 \alpha a_0^2 \omega |\langle \Psi_f^{(-)N}(k_f) | d \cdot \hat{\epsilon} | \Phi_i^N \rangle|^2, \quad (4)$$

where α is the fine-structure constant, a_0 is the Bohr radius, ω is the photon energy in atomic units, and $\hat{\epsilon}$ is the polarization vector of the ionizing light in the molecular frame. d is the molecular frame transition dipole between the initial state and a single continuum state, as a function of the ejected electron momentum k_f .

If the molecular frame cannot be recovered, Eq. (4) must be orientationally averaged and in the case of linearly polarized laser field one obtains

$$\overline{\left(\frac{d\sigma_{if}}{dk_f} \right)} = \frac{\sigma_{if}}{4\pi} [1 + \beta_{if} P_2(\cos \theta)], \quad (5)$$

TABLE I. Target CI models used in the calculation of the molecular orbitals and cationic electronic wave functions. The last column lists the maximum number of configuration state functions (CSFs) generated for a single symmetry.

Target model	Active space	CSFs
CI-1	$(1-5a')^{10}(6-17a', 1-5a'')^5$	4620
CI-2	$(1-5a')^{10}(6-18a', 1-6a'')^5$	7281
CI-3	$(1-4a')^8(6-13a', 1-3a'')^7$	11637

where β is the asymmetry parameter, σ_{if} is the partial PI cross section, P_2 is the second-order Legendre polynomial, and θ is the electron ejection angle between the photoelectron emission direction and photon polarization direction in the case of linear polarization.

B. Target model

The geometry of the HCO radical at the ground state is obtained by optimization at the second-order Møller-Plesset/augmented correlation-consistent polarized valence triple zeta (MP2/aug-cc-pVTZ) level of theory from the NIST website [13]. It has C_s symmetry with $R(\text{CO}) = 1.183 \text{ \AA}$ and $R(\text{CH}) = 1.117 \text{ \AA}$, and angle $\angle\text{HCO} = 116.9^\circ$. The Hartree-Fock electron configuration for the X^2A' ground state is given by $(1-6a')^{12}(1a'')^2(7a')^1$. In the calculations for the target, we first performed a self-consistent field (SCF) Hartree-Fock (HF) calculation for the ground state of the HCO⁺ ions in the neutral molecular geometry with the chosen basis set using the MOLPRO suite of programs [14], and obtained a set of occupied and virtual orbitals. Because the SCF method is inadequate to provide a good representation of the target states, we then improve the energy of the ground as well as the excited states by using configuration-interaction (CI) wave functions.

To select the proper basis set for the calculations, three major factors need to be considered. First, the selected basis set should be able to deliver an accurate vertical ionization potential. Second, the basis set should be small enough to be computationally tractable in conjunction with a continuum basis, when used in a scattering calculation. Finally, the target wave functions must fit inside the R -matrix sphere as this is the basic assumption of the method. In practice we avoid using the diffuse functions because they require a larger R -matrix sphere and greater computational resources. In the present work, the 6-311G* basis set is used in the target calculation.

The complete active space (CAS) CI method was used to deal with the PI process. As shown in Table I, three different CI models are used to construct target wave functions. This allowed us to investigate the role of correlation in PI. Ten electrons in the inner molecule orbitals $1-5a'$ are frozen in the CI-1 and CI-2 models. The remaining five electrons are allowed to move freely in the active space including $6-17a'$ and $1-5a''$ orbitals for the CI-1 model, while the CI-2 model extends the active space up to $18a'$ and $6a''$ orbitals. In the CI-3 model only eight electrons are frozen, which leads to very large inner region Hamiltonians. Therefore the smaller active space including $5-13a'$ and $1-3a''$ orbitals is used for the CI-3 model to make sure the scattering calculations are affordable.

TABLE II. Vertical ionization potentials (in eV) for the four lowest states of HCO^+ as obtained with Gaussian functions for continuum.

Ion state	Configuration	CI-1	CI-2 ^a	CI-3	Expt.	Theor.
X^1A'	$(7a')^{-1}$	8.70	8.65 (8.75)	9.03	9.31 ^b	
a^3A'	$(6a')^{-1}$	13.58	13.51 (13.60)	14.10	13.951 ^c	14.73 ^b
b^3A''	$(1a'')^{-1}$	14.61	14.57 (14.65)	15.13		15.79 ^b
A^1A''	$(1a'')^{-1}$	15.33	15.30 (15.40)	15.76		

^aThe mixed GTO-BTO2 continuum in parentheses.

^bFrom Ref. [15].

^cFrom Ref. [16].

The calculated vertical ionization potentials (IPs) for the first four low-lying states of HCO^+ ions are tabulated in Table II, together with the available results [15,16] for comparison. As seen from the table, both the CI-1 and CI-2 models predict very similar IPs. The CI-3 model including the largest configuration state functions (CSFs) improves the IPs to 0.3–0.5 eV, and is closest to the available data [15,16]. Our first IP of the X^1A' state varies from 8.65 to 9.03 eV, and is 0.28–0.66 eV lower than the experimental value of 9.31 eV [15]. Our second IP of 13.51–14.10 eV for the a^3A' state is in agreement with the experimental value of 13.95 eV [16]. For both a^3A' and b^3A'' states, the deviations between our result and the available theoretical result are about 0.63–1.22 eV, which is due to not enough correlation energy included in their calculations, as shown in Ref. [15]. The orbital occupation differences between the HF neutral target wave function and the principal configuration state functions (CSFs) of the ion states are also listed in Table II.

C. Inner and outer regions

In the inner region, the continuum electron is commonly represented by Gaussian-type orbitals (GTOs). Exponents of these diffuse Gaussians were obtained by the GTOBAS program [17]. As discussed in our previous paper [8], GTOs are not stable when higher values of the kinetic energy of the photoelectron and higher partial waves need to be considered. These limitations can be overcome by using B splines to represent the continuum. The corresponding BTOs have the form

$$B(r)_{i,l,m} = \frac{B_i(r)}{r} X_{lm}(\Omega), \quad (6)$$

where $B_i(r)$ is the i th radial B spline drawn from the set of B splines which are uniquely specified by the set of knots, breakpoints, and polynomial order of the B splines, and $X_{lm}(\Omega)$ is the real spherical harmonic. B splines have been used successfully in atomic calculations [18], and are becoming popular for molecular calculations [19–21]. However, greater computational resources are required in the BTO calculations. This limits their use in large molecular systems. Therefore, we test an intermediate continuum calculation, the mixed continuum bases (GTO and BTO), in the present calculations.

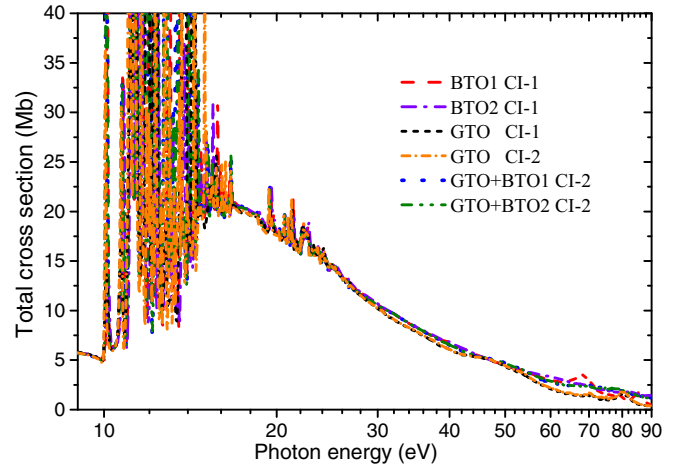


FIG. 1. Total photoionization cross sections of HCO radicals calculated with different types of continua indicated in the figure and different CI models.

For the target model using the 6-311G* basis set, an R -matrix radius of $R = 15a_0$ was sufficient to enclose the total electron density of the target inside the inner region. As a test, two sets of B -spline bases were used to access the continuum description. One set of B -spline bases named BTO1 consisted of 15 functions and order of 6, and the other one named BTO2 is of 20 functions and order of 9. The maximum angular momenta $l_{\max} = 4$ and 6 were used to check the convergence of the partial-wave expansion. The mixed GTO-BTO continuum calculations were performed with $a_{\text{GTO}} = 8a_0$ and $a_{\text{BTO}} = 7a_0$. The orthogonalization deletion threshold for GTO-only calculations was 10^{-7} . A much higher deletion threshold of 10^{-6} was applied for calculations involving the BTO. The first two radial B splines are not included in the basis due to these having a nonzero first derivative at the starting point.

In the present calculations, the L^2 configurations in Eq. (3) are written in two classes, $(\text{core})^n(\text{CAS})^{14-n}(\text{virtual})^1$ and $(\text{core})^n(\text{CAS})^{15-n}$, and here n is the number of frozen electrons. The inclusion of a large number of target states is necessary to converge the close-coupling expansion and to avoid any unphysical pseudoresonances that may otherwise appear at higher energies related to target states left out of the expansion. Forty target states was included in the close-coupling (CC) calculations, and it was enough to obtain the convergence of the close-coupling expansion. In the present calculations, the molecular orbitals (MOs) of the molecular ion are used to describe the ground-state wave function of the neutral molecule. This is an approximate method to describe the ground-state wave functions, however, it greatly simplifies evaluation of the transition dipole moments, since the same set of MOs is used in the initial- and the final-state wave functions.

III. TESTS OF MODELS

Figure 1 presents total PI cross sections of HCO radicals for calculations using GTOs and two different CI models. Increasing the two virtual orbitals in the active space of the CI-2 model does not affect the total cross section when

comparing with the CI-1 results. The two more active electrons included in the CI-3 model greatly increase the requirement of the resource. Due to the limited ability of the computer, only eight virtual molecule orbitals are considered in the CI-3 calculations. This model predicts much bigger cross sections, which is due to the inadequate description of the correlation in the model. For this reason, we do not show CI-3 results in the figure. This problem is minimized adequately in the present R -matrix calculation using a better description of the electron correlation in the CI-1 and CI-2 configurations.

The effect of an increasing number of radial B splines and order of B splines included in the CI-1 calculations on the total cross section is illustrated in Fig. 1, in which the details of the BTO1 and BTO2 results are depicted. The differences between these two BTOs is negligible in the energy region below 55 eV, while at the higher photon energy above 55 eV, the cross sections for BTO1 begin to oscillate along the cross sections for the BTO2 basis, indicating the BTO1 may not be good enough to describe the continuum states in the present energy region.

In order to access the quality of the description of the continuum, the cross sections with GTO in the CI-1 model are also shown in Fig. 1 for comparison. The total cross section obtained with BTO2 is higher than those obtained with GTO above 30 eV, and the differences between them become larger with increasing the photon energy. This indicates that the GTO may not be good enough to describe the continuum states. The results confirm the conclusions obtained by our previous PI calculations for OH radicals [8]. Here, we extend this term to a higher-energy region.

Two sets of mixed bases composed of GTO + BTO1 and GTO + BTO2 are also used in the present calculations, and their total cross sections within the CI-2 model are depicted in Fig. 1. As shown in the figure, both mixed bases predicted extremely similar results, showing that these two continuum bases produce cross sections of a similar quality. The cross sections for the GTO-only base within the CI-2 model are also collected in Fig. 1 for comparison. Large differences between the GTO base and two mixed bases again exhibit the reliability of BTO.

Figure 2 presents total PI cross sections from the ground state of HCO radicals calculated with the mixed base GTO + BTO2 for partial waves up to $l = 4$ and 6. As shown in the picture, the total cross sections of $l_{\max} = 4$ are in good agreement with those for $l_{\max} = 6$. The effect of increasing l_{\max} on the cross section is very small. The additional angular momenta contribute only slightly to the overall convergence of the cross section. This indicates that $l_{\max} = 4$ is sufficient to obtain converged PI results for HCO in the present calculations.

IV. RESULTS AND DISCUSSIONS

Inspecting the previous results, it was found that the scattering model with the mixed GTO + BTO2 continuum and the maximum angular momentum of $l_{\max} = 6$ with the CI-2 model including 40 target states represents our best model for the description of PI from HCO. The results for this model are plotted and discussed in this section.

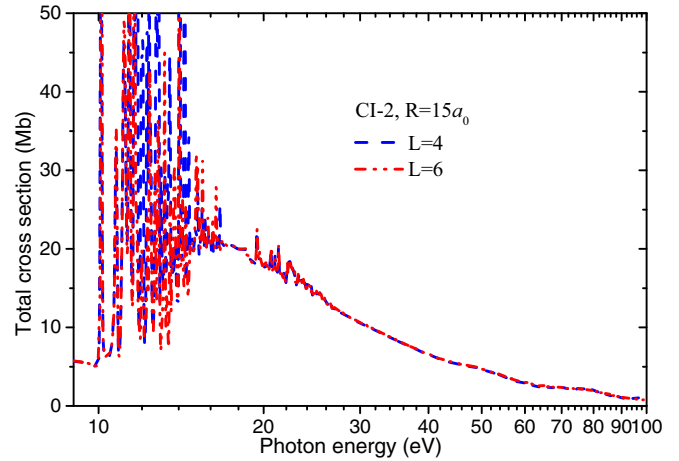


FIG. 2. Total photoionization cross sections calculated with different partial waves up to $l = 4$ and 6 for HCO radicals.

The total PI cross sections from the X^2A' ground state of HCO radicals in the energy region 8–13 eV are shown in Fig. 3, with the available experimental results for comparison. We used a fine mesh for photon energies in steps of 0.04 eV to scan and properly separate the possible resonance structures. As seen from the figure, our spectra begin from 8.75 eV, which is the value of our first vertical IP. The experimental spectra [6,22] exhibit an adiabatic ionization energy at about 8.15 eV. The large difference between them comes from the fact that the large structural relaxation occurs when one measures the adiabatic ionization energy. This can also be seen from the slow rise of the experimental PI cross section from the threshold. Our total cross sections show numerous sharp peaks originating from electron excited resonances as well as Rydberg resonances associated with the excited electronic states of the HCO^+ ion. For easier comparison, we have removed the narrow resonant features from the results obtained with the 40-state CC model by smoothing the partial-wave dipoles with a Gaussian of width 1.50 eV. Note that these

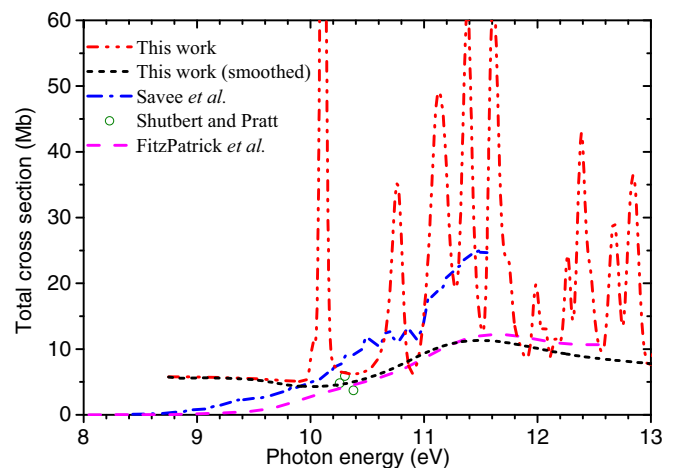


FIG. 3. Total photoionization cross sections of HCO radicals calculated with our best model in the energy range 8–13 eV, and comparison with the available experimental results.

narrow spikes ultimately are difficult to be resolved in the experiment.

The present results are in good agreement with the measured results from Shubert and Pratt [4] for the photon energies at 10.304, 10.257, and 10.379 eV. FitzPatrick *et al.* [5] measured the PI cross section of HCO between 8.0 and 12.8 eV, and set it to an absolute cross-section scale using the known cross section of ethene at 11.27 eV. As presented in Fig. 3, this measurement displays similar values of our smoothed results, especially in the energy between 10.3 and 11.3 eV.

Savee *et al.* [6] measured a PI spectrum of the HCO radical between 8 and 11.5 eV. They observed four autoionization resonances at 10.325, 10.503, 10.668, and 10.852 eV, respectively. These peaks were assigned to the autoionization of vibrationally excited $3s\sigma$ Rydberg states of HCO that converge to the a^3A' state of HCO^+ . Two resonant peaks around 10.11 and 10.76 eV are also detected in our raw spectra, which are in good agreement with the experimental results of Savee *et al.* [6]. More peaks appearing in the experimental cross section are due to the measured results including vibrational effects which are not considered in the present fixed-nuclei approximation calculations. At higher energy our result shows a significant rise starting from 11.0 eV, indicating a shape resonance may be formed. This broad peak is also detected in the experimental measurements from FitzPatrick *et al.* [5] and from Savee *et al.* [6]. It is noted that the experimental measurement of Savee *et al.* [6] agrees well with our raw spectra, but is a factor of 1.5 larger than our smoothed result above 10 eV.

Photoelectron angular distributions, along with PI cross sections, are important in structural studies of molecules. Assuming an isotropic initial state, the asymmetry parameter β completely characterizes the shape of the photoelectron emission pattern. Investigation of the asymmetry parameter near the autodetaching resonances can thus reveal the role of correlation effects in the PI process. In the following text, we will look at the calculated partial cross section and the asymmetry parameter.

Figure 4 presents the partial cross section and asymmetry parameter for PI from the ground state of HCO leading to the X^1A' state of HCO^+ ions. The present spectra (40-state CC) show a rise, which is also detected in the total cross section, starting from 11.0 eV. In order to identify the resonance and study the multichannel effects, we also carry out the one-state CC and static-exchange (SE) calculations for the PI leading to the X^1A' state of HCO^+ ions. For convenience of comparison, we smooth the partial-wave dipoles for the one-state and 40-state CC models with a Gaussian of width 1.50 eV. As shown in Fig. 4, one broad peak at 10.95 eV is found in the X^1A' cross-section profile obtained with the SE calculation, while a narrow peak is observed at 13.01 eV in the one-state CC calculation. This peak locates at 11.50 eV in the 40-state CC calculation. There is no doubt that it belongs to a shape resonance. The more states involved in the CC calculations in the 40-state model provide the necessary polarization potential in an *ab initio* way, which is crucial for determining the true resonances and their resonance parameters. In the energy region between 14 and 21 eV, the smoothed 40-state CC cross section is slightly higher than the SE result, but at

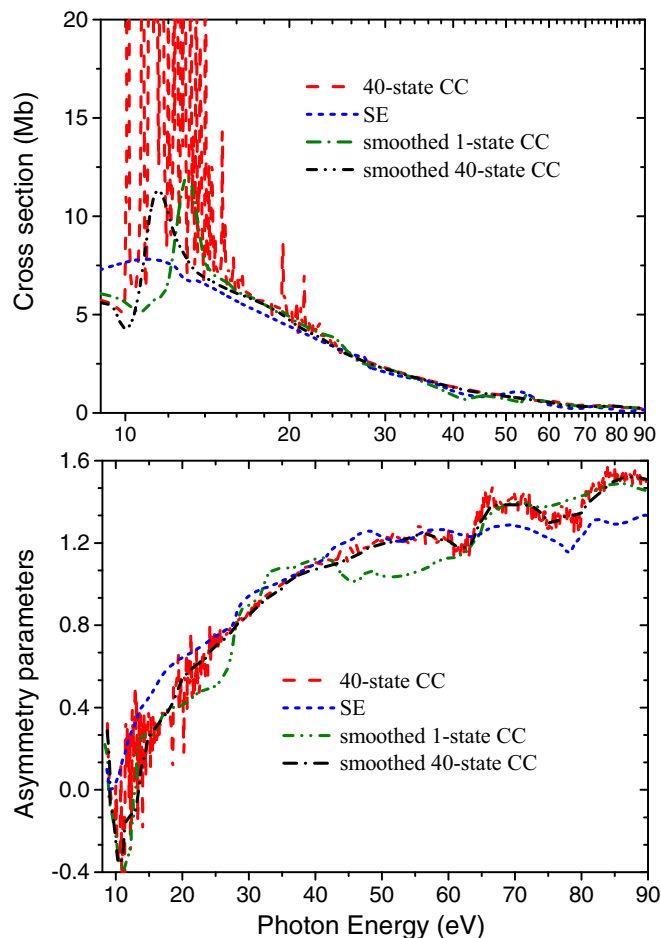


FIG. 4. Photoionization cross section and asymmetry parameter for ionization from the ground state of HCO leading to the X^1A' state of HCO^+ ions.

the higher-energy region, the differences among these three models become very small, indicating both the correlation and multichannel effects are not so important in the energy region above 21 eV.

Similar to the calculated cross section, our asymmetry parameter for ionization leading to the ionic state X^1A' from the 40-state CC model has numerous sharp peaks, as shown in Fig. 4. With respect to the behavior of the cross section, the asymmetry parameter is seen to be more affected by electron correlation effects, as can be judged from the overall large differences among these three models. The introduction of electron correlation in the initial and final ionic states causes a dramatic change in the computed asymmetry parameter, as can be seen by comparing the SE profile with our one-state CC results: The initial-state configuration interaction and final-ionic state configuration interaction cause a lowering of the computed profiles in the energy regions from threshold to 27.9 eV and between 41.6 and 63.7 eV, and an increase of the asymmetry parameter above 64.9 eV. Strong multichannel coupling effects in the 40-state CC model cause the asymmetry parameter to show large differences, compared to the one-state CC calculations.

Figure 5 presents the partial cross section and asymmetry parameter for PI from the ground state of HCO leading to the

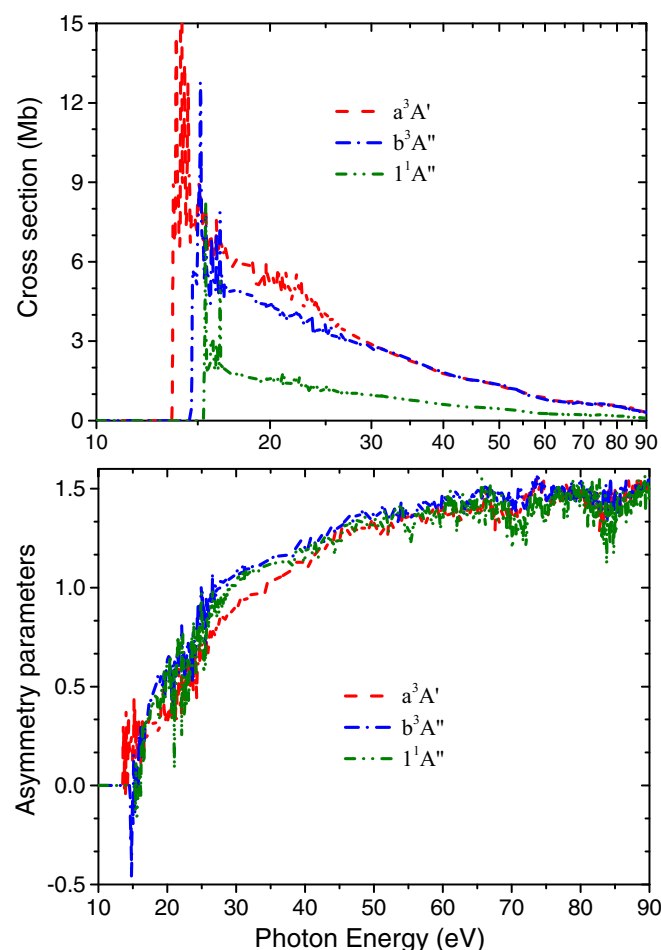


FIG. 5. Photoionization cross section and asymmetry parameter for ionization from the ground state of HCO leading to the a^3A' , b^3A'' , and A^1A'' states of HCO^+ ions.

a^3A' , b^3A'' , and A^1A'' states of HCO^+ ions. The calculations clearly indicate the complicated energy dependence of the asymmetry parameter. The sudden jumps for the asymmetry parameter are due to the corresponding resonances.

V. SUMMARY

We carried out a detailed study of the PI process for the ground state of HCO radicals, and presented predictions

for a variety of parameters, including angle-integrated cross sections, partial cross sections, the resonance structure, and the asymmetry parameter of the angular distribution. The calculations were performed with the multichannel R -matrix method, with emphasis on the convergence of the results and the accuracy of the cross sections. We took advantage of the fact that the present approach allows us to use B -spline orbitals to describe the continuum and employ the CI method to describe the electronic correlation.

Several experimental PI cross sections have been reported to date. However, these measurements show large differences. Our PI cross sections are compared with these experiments. In general, our smoothed cross section is in close agreement with the experimental measurements of FitzPatrick *et al.* [5] and Shubert and Pratt [4], but are slightly lower than the measurements from Savee *et al.* [6] in the photon energy between 10.0 and 11.8 eV. Numerous sharp autoionization resonances near the threshold are detected in our total raw cross sections. Two of these resonances around 10.11 and 10.76 eV are in good agreement with the experimental results of Savee *et al.* [6]. At higher photoelectron energies, we found a broad shape resonance located at 11.45 eV, which agreed well with a significant rise starting from 11.0 eV in the experimental spectra from Savee *et al.* [6] and from FitzPatrick *et al.* [5].

To test and verify the role played by the various types of many-body effects, one needs to measure the PI dynamical parameters, but these measurements are usually challenging, in particular for free radicals. This theoretical calculation for such a high-energy spectral region with highly accurate values of the valence-state PI cross section will help us to understand the PI dynamics of other isoelectronic molecules. The present cross sections are averaged out for all angular orientations. Hence, it gives a clear manifestation of PI cross sections. Our calculations enlighten the disagreement between the three different experimental approaches, and our cross sections will help the astrophysics community directly to model this environment.

ACKNOWLEDGMENTS

This work was supported by the Natural Science Foundation of China under Grants No. U1504109 and No. 11604085. We thank Libo Zhao for reading and improving the manuscript. This work was funded by Natural Science Foundation of Henan Province under Grant No. 212300410054, and of Henan Normal University under Grant No. 2021PL14.

-
- [1] D. J. Hucknall, *Chemistry of Hydrocarbon Combustion* (Chapman and Hall, London, 1985), and references therein.
- [2] B. J. Finlayson-Pitts and J. N. Pitts, Jr., *Atmospheric Chemistry: Fundamentals and Experimental Techniques* (Wiley and Sons, New York, 1986), and references therein.
- [3] M. Gerin, H. Liszt, D. Neufeld, B. Godard, P. Sonnentrucker, J. Pety, and E. Roueff, *Astron. Astrophys.* **622**, A26 (2019).
- [4] V. A. Shubert and S. T. Pratt, *J. Phys. Chem. A* **114**, 11238 (2010).
- [5] B. L. FitzPatrick, B. W. Alligood, L. J. Butler, S. H. Lee, and J. J. M. Lin, *J. Chem. Phys.* **133**, 094306 (2010).
- [6] J. D. Savee, B. Sztáray, O. Welz, C. A. Taatjes, and D. L. Osborn, *J. Phys. Chem. A* **125**, 3874 (2021).
- [7] Z. Mašín, J. Benda, J. D. Gorfinkiel, A. G. Harvey, and J. Tennyson, *Comput. Phys. Commun.* **249**, 107092 (2020).
- [8] K. D. Wang, J. Liu, H. X. Zhang, and Y. F. Liu, *Phys. Rev. A* **103**, 063101 (2021).
- [9] K. D. Wang, J. Liu, Y. Wang, C. J. Yang, and Y. F. Liu, *Astron. Astrophys.* **654**, A172 (2021).

- [10] P. G. Burke, *R-Matrix Theory of Atomic Collisions* (Springer, Berlin, 2011).
- [11] J. Tennyson, C. J. Noble, and P. G. Burke, *Int. J. Quantum Chem.* **29**, 1033 (1986).
- [12] A. G. Harvey, D. S. Brambila, F. Morales, and O. Smirnova, *J. Phys. B: At., Mol. Opt. Phys.* **47**, 215005 (2014).
- [13] K. P. Huber and G. Herzberg, *Constants of Diatomic Molecules* (Van Nostrand, New York, 1979).
- [14] H.-J. Werner, P. J. Knowles, G. Knizia, F. R. Manby, and M. Schütz, *WIREs Comput. Mol. Sci.* **2**, 242 (2012).
- [15] J. M. Dyke, N. B. H. Jonathan, A. Morris, and M. J. Winter, *Mol. Phys.* **39**, 629 (1980).
- [16] R. C. Fortenberry, X. C. Huang, T. D. Crawford, and T. J. Lee, *J. Phys. Chem. A* **117**, 9324 (2013).
- [17] A. Faure, J. D. Gorfinkiel, L. A. Morgan, and J. Tennyson, *Comput. Phys. Commun.* **144**, 224 (2002).
- [18] K. Wang, K. Bartschat, and O. Zatsarinny, *Astrophys. J.* **867**, 63 (2018).
- [19] C. Marante, M. Klinker, I. Corral, J. González-Vázquez, L. Argenti, and F. Martín, *J. Chem. Theory Comput.* **13**, 499 (2017).
- [20] M. Ruberti, *J. Chem. Theory Comput.* **15**, 3635 (2019).
- [21] T. Moitra, A. Ponzi, H. Koch, S. Coriani, and P. Decleva, *J. Phys. Chem. Lett.* **11**, 5330 (2020).
- [22] E. Mayer and E. R. Grant, *J. Chem. Phys.* **103**, 10513 (1995).